PRDM14 controls X-chromosomal and global epigenetic reprogramming of H3K27me3 in migrating mouse primordial germ cells

Anna Mallol[1,*], Maria Guirola[1,*] and Bernhard Payer[1,2,‡]

1. Centre for Genomic Regulation (CRG), The Barcelona Institute of Science and Technology, Dr. Aiguader 88, Barcelona 08003, Spain

2. Universitat Pompeu Fabra (UPF), Barcelona, Spain

Running Title: Role of PRDM14 in migrating PGCs

KEY WORDS: PRDM14, X-chromosome reactivation, PGCs, epigenetic reprogramming, H3K27me3, mouse

*These authors contributed equally to this work

‡Author for correspondence (bernhard.payer@crg.eu)

ORCID: A.M., 0000-0001-7366-0980; M.G., 0000-0003-1381-4567; B.P., 0000-0002-4694-2082

ABSTRACT

In order to prepare the genome for gametogenesis, primordial germ cells (PGCs) undergo extensive epigenetic reprogramming during migration towards the gonads in mammalian embryos. This includes changes on a genome-wide scale and additionally in females the remodeling of the inactive X-chromosome to enable X-chromosome reactivation (XCR). However, if global and X-chromosomal remodeling are related and which factors are important is unknown. Here we identify the germ cell determinant PR-domain containing protein 14 (PRDM14) as the first known factor that is instrumental for both global and X-chromosomal reprogramming in migrating mouse PGCs. We find that global upregulation of the repressive histone H3 lysine 27 trimethylation (H3K27me3) mark is PRDM14 dosage-dependent in PGCs of both sexes. When focusing on XCR, we observed that PRDM14 is required for removal of H3K27me3 from the inactive X-chromosome. Furthermore we show that global and X-chromosomal H3K27me3 reprogramming are functionally separable, despite their common regulation by PRDM14. Thereby we provide mechanistic insight and spatiotemporal resolution to the remodeling of the epigenome during mouse PGC migration and link epigenetic reprogramming to its developmental context *in vivo*.

INTRODUCTION

The germ cell lineage has the unique function of transmitting genetic and epigenetic information from one generation to the next. Mammalian germ cell development is an intricate process, which involves extensive changes to the epigenome before it is passed on by the gametes. In mice, germ cell development begins with specification of PGCs in the proximal epiblast. After specification, PGCs migrate through the hindgut in order to reach the genital ridges (future gonads), where they later undergo meiosis and sex-specific differentiation into eggs and sperm. During migration and colonialization of the gonads, the PGC epigenome is remodeled at multiple levels, which includes

65 global DNA-demethylation, erasure of genomic imprints, removal of histone
66 H3 lysine 9 dimethylation (H3K9me2) and a global increase of the PRC2
67 (Polycomb repressive complex 2)-associated H3K27me3 mark (Hajkova et
68 al., 2008; Leitch et al., 2013a; Reik and Surani, 2015; Saitou et al., 2012; Seki
69 et al., 2005; Seki et al., 2007). Around the same time, in female PGCs, the
70 inactive X-chromosome is reactivated by XCR, which involves downregulation
71 of the non-coding RNA Xist, the master regulator of X-inactivation, removal of
72 repressive epigenetic marks like H3K27me3 and reactivation of X-linked
73 genes (Chuva de Sousa Lopes et al., 2008; de Napoles et al., 2007; Payer,
74 2016; Sugimoto and Abe, 2007). Interestingly, H3K27me3 is therefore
75 removed from the inactive X-chromosome while it increases globally on
76 autosomes. It is currently unknown, how X-chromosomal and global
77 H3K27me3 reprogramming occur along the migration path of PGCs and if
78 they are functionally linked or are rather regulated independently of each
79 other.
80 XCR is a process linked to naïve pluripotency and germ cell fate (Pasque and
81 Plath, 2015; Payer and Lee, 2014). While XCR-kinetics have been
82 characterized during mouse and human germ cell development (Chuva de
83 Sousa Lopes et al., 2008; de Napoles et al., 2007; Guo et al., 2015; Sugimoto
84 and Abe, 2007; Tang et al., 2015), the molecular mechanisms are largely
85 unknown. Although many factors have been described, which are
86 instrumental in setting up the inactive chromatin configuration during X-
87 chromosome inactivation (Galupa and Heard, 2018; Moindrot and Brockdorff,
88 2016; Payer, 2017), little is known about the factors, which are functionally
89 important to reverse the inactive state during XCR. Identifying such X-
90 reactivation factors would be a key step towards revealing mechanistically
91 how epigenetic memory can be erased in the germ line. We and others have
92 shown that the transcriptional regulator PRDM14 plays a critical role in XCR in
93 the mouse blastocyst epiblast *in vivo* and during induced pluripotent stem cell
94 (iPSC) reprogramming (Payer et al., 2013) and epiblast stem cell (EpiSC) to
95 embryonic stem cell (ESC) conversion (Gillich et al., 2012) *in vitro*. In the
96 absence of PRDM14, downregulation of Xist and removal of the H3K27me3

97 mark from the inactive X-chromosome are perturbed, likely due to repressive
98 functions of PRDM14 on *Xist* and its activator *Rnf12/Rlim* (Ma et al., 2011;
99 Payer et al., 2013).
100 Besides being important for naïve pluripotency (Yamaji et al., 2013) and the
101 associated XCR, PRDM14 is also critical for germ cell development. *Prdm14*-
102 mutant mouse embryos show reduced PGC numbers (Yamaji et al., 2008),
103 and overexpression of PRDM14 in epiblast-like cells (EpiLCs) is sufficient to
104 induce germ cell fate *in vitro* (Nakaki et al., 2013a). Importantly, PRDM14 is a
105 regulator of global epigenetic changes both in pluripotent stem cells as well as
106 in PGCs (Nakaki et al., 2013b; Seki, 2018). In particular, it has been shown
107 that PRDM14 is responsible for the low global DNA-methylation levels
108 characteristic of naïve pluripotent stem cells and PGCs, both by repressing
109 DNA-methyltransferase genes, as well as by recruiting DNA-demethylases of
110 the Ten-eleven translocation (TET) family (Ficz et al., 2013; Grabole et al.,
111 2013; Leitch et al., 2013b; Okashita et al., 2014; Yamaji et al., 2008; Yamaji et
112 al., 2013). Besides controlling DNA-hypomethylation, PRDM14 is also
113 important for global remodeling of histone marks in pluripotent stem cells and
114 PGCs. During mouse preimplantation development, PRDM14 shows
115 asymmetric expression in blastomeres of the 4-cell embryo and has been
116 implicated in driving cells towards inner cell mass fate by recruiting CARM1, a
117 histone H3 arginine 26 (H3R26me2) methyltransferase (Burton et al., 2013).
118 In migrating PGCs, *Prdm14*-mutant mouse embryos fail to downregulate the
119 repressive H3K9me2 mark and its associated histone methyltransferase
120 GLP/EHMT1 (Yamaji et al., 2008), most likely because *Glp/Ehmt1* is a directly
121 repressed target gene of PRDM14 (Tu et al., 2016). The PGC-specific
122 upregulation of H3K27me3 on a global level is also impaired in *Prdm14-/-*
123 embryos (Yamaji et al., 2008) and genome-wide distribution of H3K27me3 is
124 misregulated in *Prdm14-/-* ESCs (Yamaji et al., 2013).
125 Despite the known importance of PRDM14 for epigenetic remodeling in the
126 germ cell lineage, how PRDM14 controls its different aspects *in vivo* is largely
127 unresolved: For example, it remains unknown, if PRDM14 is important for X-
128 chromosome reactivation also in female PGCs, and if this is coordinated with

129 genome-wide epigenetic changes occurring at that time. Furthermore no
130 information is available about the spatial distribution of germ cells along their
131 migration path towards the gonads during epigenetic reprogramming. To
132 address these questions, we investigated in this study epigenetic remodeling
133 of the polycomb-associated H3K27me3 mark and its dependency on
134 PRDM14 in migrating mouse PGCs. By using a whole-mount embryo staining
135 approach, we were able for the first time to collect spatiotemporal information
136 about the epigenetic reprogramming process in mouse PGCs in relation to
137 their migratory progress. We found that PRDM14 is critical both for X-
138 chromosomal removal as well as global upregulation of H3K27me3 in PGCs.
139 We furthermore find differences in PRDM14-dosage dependence and kinetics
140 of X-chromosomal and global H3K27me3 changes. While both events are
141 controlled by PRDM14, they do not depend on each other and therefore must
142 be regulated through different mechanisms. In summary, we describe here
143 how PRDM14 regulates key aspects of epigenetic changes in germ cells and
144 how this is linked with progression of germ cell migration and development.
145
146
147 **RESULTS AND DISCUSSION**
148
149 **PRDM14 controls number and local distribution of PGCs during their**
150 **migration**
151 To address the function of PRDM14 for PGC number and migration, we
152 immunostained whole mount embryonic day (E)9.5 mouse embryos from
153 *Prdm14*$^{+/-}$ x *Prdm14*$^{+/-}$ heterozygous crosses for AP2γ, a specific marker and
154 critical factor for PGC development (Nakaki et al., 2013a; Weber et al., 2010).
155 We found that migrating PGCs at this stage were spread throughout the
156 hindgut, and observed in *Prdm14*$^{-/-}$ embryos a strong depletion of PGCs or
157 even their absence (7/17 embryos), when compared to wildtype and
158 heterozygous littermates (Fig. 1A, S1, Table S1), which is consistent with a
159 previous study of this mouse line (Yamaji et al., 2008). Generally, PGC
160 numbers increased with developmental progression (somite number) in

161 *Prdm14*$^{+/+}$ and *Prdm14*$^{+/-}$ embryos, while it remained low in *Prdm14*$^{-/-}$ embryos
162 (Fig. 1B). This is not due to a general developmental delay of *Prdm14*-mutant
163 embryos at E9.5, as somite numbers were similar between different *Prdm14*
164 genotypes (Fig. S2A, Table S1).
165 In order to analyze the distribution of PGCs in more detail, we divided the
166 migration path along the hindgut into 4 quadrants (Fig. 1C); starting with
167 quadrant 1 (Q1) at the posterior end at the base of the allantois and finishing
168 with quadrant 4 (Q4) near the area where PGCs would exit the hindgut and
169 enter the genital ridges (future gonads). At E9.5, PGCs would be found mostly
170 in Q2 and Q3 in *Prdm14*$^{+/+}$ and *Prdm14*$^{+/-}$ embryos, while PGCs in *Prdm14*$^{-/-}$
171 embryos would be located predominantly in Q1 and Q2 (Fig. 1D, S2B). This
172 indicates that *Prdm14*-mutant PGCs might be delayed in migration, although
173 few of them can be also found in Q3 and Q4. In summary, *Prdm14*-mutant
174 embryos show a strong reduction in PGC-numbers and a defect in PGC
175 migration.
176
177 **PRDM14 is required for global upregulation of H3K27me3 in migrating**
178 **PGCs**
179 As PRDM14 has a role in the global epigenetic reprogramming occurring in
180 PGCs (Yamaji et al., 2008), we wanted to investigate in more detail its
181 function for upregulating the H3K27me3 mark, which is a hallmark of
182 migrating PGCs (Hajkova et al., 2008; Seki et al., 2005; Seki et al., 2007). We
183 therefore costained E9.5 embryos of different *Prdm14* genotypes with AP2γ
184 and H3K27me3 antibodies (Fig. 2A). We scored H3K27me3 as being
185 upregulated or non-upregulated in AP2γ-positive PGCs when compared to
186 surrounding somatic cells. It thereby became apparent that H3K27me3
187 upregulation was in direct relation to PRDM14 dosage, as about 78% of
188 wildtype PGCs had elevated H3K27me3 staining, while only 54% of
189 heterozygote and only 19% of Prdm14-null PGCs did (Fig. 2B, Table S1).
190 These differences were observed to a similar degree both in male and in
191 female embryos, indicating that PRDM14 controlled global H3K27me3 levels
192 in a sex-independent manner.

193 When we assessed H3K27me3 upregulation in relation to developmental
194 progression (somite number) at E9.5, we observed that H3K27me3 increased
195 with somite number in *Prdm14*$^{+/+}$ and *Prdm14*$^{+/-}$, but not in *Prdm14*$^{-/-}$ embryos
196 (Fig. 2C). Interestingly, H3K27me3 levels did not seem to vastly change in
197 PGCs within different quadrants of their migration path, indicating that global
198 H3K27me3 upregulation depends more on overall developmental progression
199 of the embryo than on the position of the PGCs along the hindgut (Fig. S3).
200 Overall, we conclude that global H3K27me3 upregulation in PGCs is
201 dependent on PRDM14 dosage and progresses with developmental stage at
202 equal rate in both sexes.
203
204 **X-chromosomal H3K27me3-erasure during XCR in female PGCs is**
205 **dependent on PRDM14**
206
207 In contrast to the global increase of H3K27me3, stands the erasure of
208 H3K27me3 from the inactive X-chromosome in female PGCs during the
209 process of XCR (Chuva de Sousa Lopes et al., 2008; de Napoles et al.,
210 2007). As these events occur around the same time and as XCR is controlled
211 by PRDM14 in mouse blastocysts and during iPSC reprogramming (Payer et
212 al., 2013), we wanted to know if PRDM14 is also required for XCR in PGCs.
213 Thus we scored the disappearance of the distinctive H3K27me3 accumulation
214 from the inactive X-chromosome ("H3K27me3-spot") in female PGCs in
215 embryos of different *Prdm14* genotypes (Fig. 3A). While about half of both
216 *Prdm14* wildtype (52%) and heterozygous (51%) PGCs have erased the
217 H3K27me3-spot from the X, only around 23% of *Prdm14*-mutant PGCs have
218 lost the spot at E9.5 (Fig. 3B, Table S1). The erasure of the H3K27me3 spot
219 occurred progressively in *Prdm14*$^{+/+}$ and *Prdm14*$^{+/-}$ PGCs during their
220 migration along the hindgut, but did not increase with migration in *Prdm14*$^{-/-}$
221 PGCs (Fig. 3C). In contrast to global H3K27me3 upregulation, removal of the
222 X-chromosomal H3K27me3-spot therefore did not seem to be PRDM14-dose
223 dependent and did not change substantially between E9.5 embryos of
224 different somite number (Fig. S4). Taken together, our results show that

225 similar to its role in the pluripotent epiblast and during iPSC reprogramming
226 (Payer et al., 2013), PRDM14 is also a key factor for XCR in PGCs by
227 promoting the loss of the X-chromosomal H3K27me3 mark.
228
229 **X-chromosomal and global H3K27me3 reprogramming occur**
230 **independently in female PGCs**
231 H3K27me3 and its associated enzymatic complex, PRC2, are strongly
232 enriched on the inactive X-chromosome in female cells. Therefore, we
233 hypothesized, if this could act as a "sink" for PRC2, whereby global
234 upregulation of H3K27me3 in PGCs would require first stripping PRC2 off the
235 X-chromosome through XCR to make it available for acting elsewhere in the
236 genome. In order to test this hypothesis, we investigated the relationship
237 between X-chromosomal downregulation and global upregulation of
238 H3K27me3 in female PGCs (Fig. 4, S5). If the inactive X were acting as a sink
239 for PRC2, we would expect global H3K27me3 not to be upregulated in PGCs
240 harboring an X-spot. However, when comparing within the different genotypes
241 the fraction of PGCs which have lost or retained the X-chromosomal
242 H3K27me3-spot, we did not detect any significant differences in global
243 H3K27me3 upregulation (Fig. 4A). This indicates that losing the X-spot is not
244 a general prerequisite for global H3K27me3 upregulation in female PGCs.
245 Also the fact that *Prdm14*$^{+/+}$ and *Prdm14*$^{+/-}$ PGCs showed almost identical X-
246 spot loss (52% in +/+ vs. 51% in +/-) but different global H3K27me3
247 upregulation levels (75% in +/+ vs. 56% in +/-), indicates that X-spot loss and
248 global H3K27me3 upregulation are independent epigenetic events. In
249 conclusion, while PRDM14 is both required for normal X-chromosomal and
250 global H3K27me3 reprogramming in PGCs (Fig. 4B, S6), these events are
251 mechanistically separable and do not depend on each other.
252
253 **Summary and discussion**
254 In this study, we have investigated the role of PRDM14 during epigenetic
255 reprogramming in migrating mouse PGCs (summarized in Fig. 4B, S6). We
256 thereby have uncovered multiple roles for PRDM14 during germ cell

257 development. Most importantly, we have identified PRDM14 to our knowledge
258 as the first factor with functional importance for XCR in the germ cell lineage.
259 In particular, we found that erasure of H3K27me3 mark from the inactive X-
260 chromosome, a key step during X-reactivation (Borensztein et al., 2017;
261 Chuva de Sousa Lopes et al., 2008; de Napoles et al., 2007; Mak et al.,
262 2004), occurred progressively during the migration of female PGCs and
263 required PRDM14. This observation is in line with the role of PRDM14 during
264 X-reactivation in the mouse blastocyst and during iPSC-reprogramming
265 (Payer et al., 2013).
266 Second, we uncovered that global H3K27me3 upregulation in PGCs is
267 dependent on PRDM14 in a dosage-sensitive manner, as *Prdm14*$^{+/-}$ and
268 *Prdm14*$^{-/-}$ PGCs showed a progressive defect. Interestingly, we observed that
269 H3K27me3 upregulation seemed to mostly depend on the developmental
270 stage of the embryo rather than the PGC position along the migratory path,
271 which is in contrast to the kinetics of X-specific H3K27me3 removal.
272 Another key finding from our study is that the global upregulation and X-
273 chromosomal depletion of the H3K27me3 mark seem to be controlled by
274 distinct mechanisms despite their common dependency on PRDM14. This is
275 based on several observations: First, global H3K27me3 upregulation is
276 sensitive to PRDM14 dosage, while X-specific H3K27me3 removal is not.
277 Second, global upregulation correlates with embryonic stage (somite number),
278 while X-chromosomal H3K27me3 loss occurs progressively during PGC
279 migration. Third, global H3K27me3 upregulation occurs with similar kinetics in
280 male and female embryos and is affected to a similar extent by loss of
281 PRDM14 in both sexes. Finally, X-chromosomal depletion of H3K27me3 does
282 not seem to be required for global H3K27me3 upregulation on a single-cell
283 level. How then could PRDM14 control H3K27me3 remodeling on autosomes
284 versus on the X-chromosome? On the global scale, previous studies
285 suggested that PRDM14 could directly interact with the PRC2 complex in
286 pluripotent stem cells and thereby facilitate its recruitment to PRDM14 target
287 genes (Chan et al., 2013; Yamaji et al., 2013) or that PRDM14 could activate
288 expression of the PRC2 component *Suz12* (Grabole et al., 2013). More recent

289 studies however challenged this view and proposed that PRDM14 mainly acts
290 though its binding partner and co-repressor CBFA2T2/MTGR1 (Kawaguchi et
291 al., 2019; Nady et al., 2015; Tu et al., 2016), suggesting that PRC2 might be
292 recruited secondarily to PRDM14 targets. Regarding its X-chromosome-
293 specific role, we have previously shown that PRDM14 binds to regulatory
294 regions at *Xist* intron 1 and upstream of the *Xist*-activator *Rnf12* (Payer et al.,
295 2013) and thereby facilitates repression of *Xist* during XCR. As H3K27me3-
296 accumulation on the X-chromosome is *Xist*-dependent (Plath et al., 2003;
297 Schoeftner et al., 2006; Silva et al., 2003; Zhao et al., 2008), PRDM14 might
298 thereby regulate X-chromosomal H3K27me3-depletion by downregulating
299 *Xist*. The fact that H3K27me3-removal from the X-chromosome occurs
300 progressively in PGCs along their migration path, could speak in favor of a
301 cell-proliferation and replication-dependent, passive dilution mechanism,
302 similar as it has been proposed for global DNA-demethylation in PGCs
303 (Kagiwada et al., 2013; Seisenberger et al., 2012). Nevertheless, also active
304 mechanisms could play a role like removal of the mark by the H3K27me3-
305 demethylase KDM6A/UTX, which has a partial effect on H3K27me3-
306 demethylation during XCR in mouse blastocysts (Borensztein et al., 2017).
307 Finally, we have found that *Prdm14*$^{-/-}$ embryos displayed severely
308 compromised germ cell numbers as reported previously (Yamaji et al., 2008)
309 and a delay in PGC migration. This is in line with a recent study (Cheetham et
310 al., 2018), which found that genes implicated in cell migration are bound by
311 PRDM14 in PGC-like cells derived *in vitro*, suggesting that PRDM14 might be
312 directly involved in controlling PGC migration.
313 In summary, here we have shown that autosomal and X-chromosomal
314 reprogramming of H3K27me3 occur independently during PGC migration, but
315 that they rely both on the key germ cell factor PRDM14. By adding to our
316 understanding of the mechanisms underlying epigenetic changes required for
317 germ cell development *in vivo*, we provide a framework for assessing and
318 improving the quality of *in vitro*-derived gametes.
319
320

MATERIALS AND METHODS

Embryo isolation

Mouse care and procedures were conducted according to the protocols approved by the Ethics Committee on Animal Research of the Parc de Recerca Biomèdica de Barcelona (PRBB) and by the Departament de Territori i Sostenibilitat of the Generalitat de Catalunya.
Prdm14 mutant mice (Yamaji et al., 2008) were maintained in a predominant C57BL/6 strain background. *Prdm14* heterozygous mice were mated and resulting embryos were harvested from pregnant females at E9.5 and dissected from maternal tissues.

Whole mount immunostaining

The whole mount embryo immunostaining was performed as described in (Yamaji et al., 2008). The primary antibodies used were rabbit polyclonal anti-AP2γ (TCFAP2C) (Santa Cruz Biotechnology sc-8977) and mouse monoclonal anti-H3K27me3 (Active Motif 61707, clone MABI0323). The secondary antibodies used were donkey anti-rabbit IgG Alexa Fluor 488 and goat anti-mouse IgG Alexa Fluor 555 (Molecular Probes A21206 and A21424).
After the immunostaining, the somite number of every embryo was counted under the stereomicroscope. Then the embryo was split in two parts: the head was used for genotyping and the hindgut was dissected and mounted in Vectashield (Vector Laboratories) for observation with confocal microscopy.

Image capture and analysis

Bright field images of the whole embryos were captured on a stereomicroscope using the Leica application suite software (Leica Microsystems, Wetzlar, Germany). Fluorescence imaging of the hindguts was performed on an inverted Leica TCS SP5 confocal microscope using the Leica Application Suite Advanced Fluorescence software. Z-stack images (1.5

352 µm intervals) of the full hindgut were acquired. Color setting and image
353 processing were performed in Fiji (Schindelin et al., 2012) and Volocity
354 (PerkinElmer) software.
355 The location in the hindgut and both the H3K27me3 global levels and the
356 presence of the X-spot of every AP2γ positive cell were recorded. The global
357 nuclear intensity of H3K27me3 staining was classified as "upregulated" or
358 "non-upregulated" after comparing it with the staining intensity of the
359 surrounding somatic cells in the same focus plane. The total length of the
360 hindgut was divided in four quadrants (Q1-Q4 from the tail tip to the genital
361 ridges, Figure 1C) to ease the analysis of the location of AP2γ positive cells.

362

363 ***Prdm14* and sex genotyping**

364 *Prdm14* genotype was determined by polymerase chain reaction after image
365 analysis. Primer sequences are detailed in (Yamaji et al., 2008).
366 The sex of the embryo was determined by the presence of the H3K27me3
367 spot corresponding to the silent X chromosome in somatic cells of female
368 embryos (Plath et al., 2003).

369

370 **Statistical analysis**

371 Several E9.5 litters were collected and the results from all embryos were
372 pooled and analyzed with IBM SPSS Statistics software. For qualitative
373 variables χ^2 test was used, and for quantitative variables the non-parametric
374 Kruskal–Wallis test was used. Pairwise comparisons with Bonferroni's
375 correction were performed using the Mann–Whitney U test. For lineal
376 regression modeling, R^2 coefficient was calculated. In all cases, $p<0.05$ was
377 considered statistically significant.

378

379

Acknowledgements

We thank members of the Payer lab for discussions and suggestions. We thank Mitinori Saitou for sharing the *Prdm14-KO* mouse strain and for advice on whole mount detection of PGCs by immunostaining. We also thank Guillaume Filion for critical reading and advice on statistical analysis. We thank the PRBB Animal Facility for mouse husbandry, the CRG Media kitchen for reagent preparation and the CRG Advanced Light Microscopy Unit for imaging support.

Competing interests

The authors declare no competing or financial interest.

Author contributions

Conceptualization and project design: A.M., M.G., B.P.; Experimental execution: A.M., M.G.; Data Collection: A.M., M.G.; Statistical Analysis A.M.; Writing: A.M., P.B.; Supervision + Funding Acquisition: B.P.

Funding

This work has been funded by the Spanish Ministry of Science, Innovation and Universities (BFU2014-55275-P and BFU2017-88407-P), the AXA Research Fund and the Agencia de Gestio d'Ajuts Universitaris i de Recerca (AGAUR, 2017 SGR 346). We would like to thank the Spanish Ministry of Economy, Industry and Competitiveness (MEIC) to the EMBL partnership and to the 'Centro de Excelencia Severo Ochoa'. We also acknowledge support of the CERCA Programme of the Generalitat de Catalunya.

412 **References**

413

414 **Borensztein, M., Okamoto, I., Syx, L., Guilbaud, G., Picard, C., Ancelin,**
415 **K., Galupa, R., Diabangouaya, P., Servant, N., Barillot, E., et al.**
416 (2017). Contribution of epigenetic landscapes and transcription factors to
417 X-chromosome reactivation in the inner cell mass. *Nat. Commun.* **8**,
418 1297.

419 **Burton, A., Muller, J., Tu, S., Padilla-Longoria, P., Guccione, E. and**
420 **Torres-Padilla, M.-E.** (2013). Single-cell profiling of epigenetic modifiers
421 identifies PRDM14 as an inducer of cell fate in the mammalian embryo.
422 *Cell Rep.* **5**, 687–701.

423 **Chan, Y.-S., Göke, J., Lu, X., Venkatesan, N., Feng, B., Su, I.-H. and Ng,**
424 **H.-H.** (2013). A PRC2-dependent repressive role of PRDM14 in human
425 embryonic stem cells and induced pluripotent stem cell reprogramming.
426 *Stem Cells* **31**, 682–92.

427 **Cheetham, S. W., Gruhn, W. H., van den Ameele, J., Krautz, R., Southall,**
428 **T. D., Kobayashi, T., Surani, M. A. and Brand, A. H.** (2018). Targeted
429 DamID reveals differential binding of mammalian pluripotency factors.
430 *Development* **145**, dev170209.

431 **Chuva de Sousa Lopes, S. M., Hayashi, K., Shovlin, T. C., Mifsud, W.,**
432 **Surani, M. A. and McLaren, A.** (2008). X chromosome activity in mouse
433 XX primordial germ cells. *PLoS Genet.* **4**, e30.

434 **de Napoles, M., Nesterova, T. and Brockdorff, N.** (2007). Early loss of Xist
435 RNA expression and inactive X chromosome associated chromatin
436 modification in developing primordial germ cells. *PLoS One* **2**, e860.

437 **Ficz, G., Hore, T. A., Santos, F., Lee, H. J., Dean, W., Arand, J., Krueger,**
438 **F., Oxley, D., Paul, Y.-L., Walter, J., et al.** (2013). FGF signaling
439 inhibition in ESCs drives rapid genome-wide demethylation to the
440 epigenetic ground state of pluripotency. *Cell Stem Cell* **13**, 351–9.

441 **Galupa, R. and Heard, E.** (2018). X-Chromosome Inactivation: A Crossroads
442 Between Chromosome Architecture and Gene Regulation. *Annu. Rev.*
443 *Genet.* **52**, 535–566.

444 **Gillich, A., Bao, S., Grabole, N., Hayashi, K., Trotter, M. W. B., Pasque,**
445 **V., Magnúsdóttir, E. and Surani, M. A.** (2012). Epiblast stem cell-based
446 system reveals reprogramming synergy of germline factors. *Cell Stem*
447 *Cell* **10**, 425–39.
448 **Grabole, N., Tischler, J., Hackett, J. A., Kim, S., Tang, F., Leitch, H. G.,**
449 **Magnúsdóttir, E. and Surani, M. A.** (2013). Prdm14 promotes germline
450 fate and naive pluripotency by repressing FGF signalling and DNA
451 methylation. *EMBO Rep.* **14**, 629–37.
452 **Guo, F., Yan, L., Guo, H., Li, L., Hu, B., Zhao, Y., Yong, J., Hu, Y., Wang,**
453 **X., Wei, Y., et al.** (2015). The Transcriptome and DNA Methylome
454 Landscapes of Human Primordial Germ Cells. *Cell* **161**, 1437–1452.
455 **Hajkova, P., Ancelin, K., Waldmann, T., Lacoste, N., Lange, U. C., Cesari,**
456 **F., Lee, C., Almouzni, G., Schneider, R. and Surani, M. A.** (2008).
457 Chromatin dynamics during epigenetic reprogramming in the mouse germ
458 line. *Nature* **452**, 877–881.
459 **Kagiwada, S., Kurimoto, K., Hirota, T., Yamaji, M. and Saitou, M.** (2013).
460 Replication-coupled passive DNA demethylation for the erasure of
461 genome imprints in mice. *EMBO J.* **32**, 340–53.
462 **Kawaguchi, M., Sugiyama, K., Matsubara, K., Lin, C.-Y., Kuraku, S.,**
463 **Hashimoto, S., Suwa, Y., Yong, L. W., Takino, K., Higashida, S., et al.**
464 (2019). Co-option of the PRDM14-CBFA2T complex from motor neurons
465 to pluripotent cells during vertebrate evolution. *Development* **146**,.
466 **Leitch, H. G., Tang, W. W. C. and Surani, M. A.** (2013a). Primordial germ-
467 cell development and epigenetic reprogramming in mammals. *Curr. Top.*
468 *Dev. Biol.* **104**, 149–87.
469 **Leitch, H. G., Mcewen, K. R., Turp, A., Encheva, V., Carroll, T., Grabole,**
470 **N., Mansfield, W., Nashun, B., Knezovich, J. G., Smith, A., et al.**
471 (2013b). Naive pluripotency is associated with global DNA
472 hypomethylation. *Nat. Struct. Mol. Biol.* **20**, 311–316.
473 **Ma, Z., Swigut, T., Valouev, A., Rada-Iglesias, A. and Wysocka, J.** (2011).
474 Sequence-specific regulator Prdm14 safeguards mouse ESCs from
475 entering extraembryonic endoderm fates. *Nat. Struct. Mol. Biol.* **18**, 120–

476 7.
477 **Mak, W., Nesterova, T. B., de Napoles, M., Appanah, R., Yamanaka, S.,**
478 **Otte, A. P. and Brockdorff, N.** (2004). Reactivation of the paternal X
479 chromosome in early mouse embryos. *Science* **303**, 666–9.
480 **Moindrot, B. and Brockdorff, N.** (2016). RNA binding proteins implicated in
481 Xist-mediated chromosome silencing. *Semin. Cell Dev. Biol.* **56**, 58–70.
482 **Nady, N., Gupta, A., Ma, Z., Swigut, T., Koide, A., Koide, S. and Wysocka,**
483 **J.** (2015). ETO family protein Mtgr1 mediates Prdm14 functions in stem
484 cell maintenance and primordial germ cell formation. *Elife* **4**, e10150.
485 **Nakaki, F., Hayashi, K., Ohta, H., Kurimoto, K., Yabuta, Y. and Saitou, M.**
486 (2013a). Induction of mouse germ-cell fate by transcription factors in
487 vitro. *Nature* **501**, 222–6.
488 **Nakaki, F., Hayashi, K., Ohta, H., Kurimoto, K., Yabuta, Y. and Saitou, M.**
489 (2013b). Induction of mouse germ-cell fate by transcription factors in
490 vitro. *Nature* **501**, 222–6.
491 **Okashita, N., Kumaki, Y., Ebi, K., Nishi, M., Okamoto, Y., Nakayama, M.,**
492 **Hashimoto, S., Nakamura, T., Sugasawa, K., Kojima, N., et al.** (2014).
493 PRDM14 promotes active DNA demethylation through the ten-eleven
494 translocation (TET)-mediated base excision repair pathway in embryonic
495 stem cells. *Development* **141**, 269–80.
496 **Pasque, V. and Plath, K.** (2015). X chromosome reactivation in
497 reprogramming and in development. *Curr. Opin. Cell Biol.* **37**, 75–83.
498 **Payer, B.** (2016). Developmental regulation of X-chromosome inactivation.
499 *Semin. Cell Dev. Biol.* **56**, 88–99.
500 **Payer, B.** (2017). Epigenetic Regulation of X-Chromosome Inactivation. In
501 *Epigenetics in Human Reproduction and Development*, pp. 113–158.
502 World Scientific Publishing.
503 **Payer, B. and Lee, J. T.** (2014). Coupling of X-Chromosome reactivation with
504 the pluripotent stem cell state. *RNA Biol.* **11**, 798–807.
505 **Payer, B., Rosenberg, M., Yamaji, M., Yabuta, Y., Koyanagi-Aoi, M.,**
506 **Hayashi, K., Yamanaka, S., Saitou, M. and Lee, J. T.** (2013). Tsix RNA
507 and the germline factor, PRDM14, link X reactivation and stem cell

508 reprogramming. *Mol. Cell* **52**, 805–18.
509 **Plath, K., Fang, J., Mlynarczyk-Evans, S. K., Cao, R., Worringer, K. A.,**
510 **Wang, H., de la Cruz, C. C., Otte, A. P., Panning, B. and Zhang, Y.**
511 (2003). Role of histone H3 lysine 27 methylation in X inactivation.
512 *Science* **300**, 131–5.
513 **Reik, W. and Surani, M. A.** (2015). Germline and Pluripotent Stem Cells.
514 *Cold Spring Harb. Perspect. Biol.* **7**, 1–24.
515 **Saitou, M., Kagiwada, S. and Kurimoto, K.** (2012). Epigenetic
516 reprogramming in mouse pre-implantation development and primordial
517 germ cells. *Development* **139**, 15–31.
518 **Schindelin, J., Arganda-Carreras, I., Frise, E., Kaynig, V., Longair, M.,**
519 **Pietzsch, T., Preibisch, S., Rueden, C., Saalfeld, S., Schmid, B., et al.**
520 (2012). Fiji: An open-source platform for biological-image analysis. *Nat.*
521 *Methods* **9**, 676–682.
522 **Schoeftner, S., Sengupta, A. K., Kubicek, S., Mechtler, K., Spahn, L.,**
523 **Koseki, H., Jenuwein, T. and Wutz, A.** (2006). Recruitment of PRC1
524 function at the initiation of X inactivation independent of PRC2 and
525 silencing. *EMBO J.* **25**, 3110–22.
526 **Seisenberger, S., Andrews, S., Krueger, F., Arand, J., Walter, J., Santos,**
527 **F., Popp, C., Thienpont, B., Dean, W. and Reik, W.** (2012). The
528 dynamics of genome-wide DNA methylation reprogramming in mouse
529 primordial germ cells. *Mol. Cell* **48**, 849–62.
530 **Seki, Y.** (2018). PRDM14 Is a Unique Epigenetic Regulator Stabilizing
531 Transcriptional Networks for Pluripotency. *Front. cell Dev. Biol.* **6**, 12.
532 **Seki, Y., Hayashi, K., Itoh, K., Mizugaki, M., Saitou, M. and Matsui, Y.**
533 (2005). Extensive and orderly reprogramming of genome-wide chromatin
534 modifications associated with specification and early development of
535 germ cells in mice. *Dev. Biol.* **278**, 440–58.
536 **Seki, Y., Yamaji, M., Yabuta, Y., Sano, M., Shigeta, M., Matsui, Y., Saga,**
537 **Y., Tachibana, M., Shinkai, Y. and Saitou, M.** (2007). Cellular dynamics
538 associated with the genome-wide epigenetic reprogramming in migrating
539 primordial germ cells in mice. *Development* **134**, 2627–38.

540 **Silva, J. C. R., Mak, W., Zvetkova, I., Appanah, R., Nesterova, T. B.,**
541 **Webster, Z., Peters, A., Jenuwein, T., Otte, A. P. and Brockdorff, N.**
542 (2003). Establishment of histone h3 methylation on the inactive X
543 chromosome requires transient recruitment of Eed-Enx1 polycomb group
544 complexes. *Dev. Cell* **4**, 481–495.
545 **Sugimoto, M. and Abe, K.** (2007). X chromosome reactivation initiates in
546 nascent primordial germ cells in mice. *PLoS Genet.* **3**, e116.
547 **Tang, W. W. C., Dietmann, S., Irie, N., Leitch, H. G., Floros, V. I.,**
548 **Bradshaw, C. R., Hackett, J. A., Chinnery, P. F. and Surani, M. A.**
549 (2015). A Unique Gene Regulatory Network Resets the Human Germline
550 Epigenome for Development. *Cell* **161**, 1453–1467.
551 **Tu, S., Narendra, V., Yamaji, M., Vidal, S. E., Rojas, L. A., Wang, X., Kim,**
552 **S. Y., Garcia, B. A., Tuschl, T., Stadtfeld, M., et al.** (2016). Co-
553 repressor CBFA2T2 regulates pluripotency and germline development.
554 *Nature* **534**, 387–90.
555 **Weber, S., Eckert, D., Nettersheim, D., Gillis, A. J. M., Schäfer, S.,**
556 **Kuckenberg, P., Ehlermann, J., Werling, U., Biermann, K., Looijenga,**
557 **L. H. J., et al.** (2010). Critical function of AP-2 gamma/TCFAP2C in
558 mouse embryonic germ cell maintenance. *Biol. Reprod.* **82**, 214–23.
559 **Yamaji, M., Seki, Y., Kurimoto, K., Yabuta, Y., Yuasa, M., Shigeta, M.,**
560 **Yamanaka, K., Ohinata, Y. and Saitou, M.** (2008). Critical function of
561 Prdm14 for the establishment of the germ cell lineage in mice. *Nat.*
562 *Genet.* **40**, 1016–22.
563 **Yamaji, M., Ueda, J., Hayashi, K., Ohta, H., Yabuta, Y., Kurimoto, K.,**
564 **Nakato, R., Yamada, Y., Shirahige, K. and Saitou, M.** (2013). PRDM14
565 ensures naive pluripotency through dual regulation of signaling and
566 epigenetic pathways in mouse embryonic stem cells. *Cell Stem Cell* **12**,
567 368–82.
568 **Zhao, J., Sun, B. K., Erwin, J. A., Song, J.-J. and Lee, J. T.** (2008).
569 Polycomb proteins targeted by a short repeat RNA to the mouse X
570 chromosome. *Science* **322**, 750–6.
571

572

573 **FIGURE LEGENDS**

574

575 **Fig. 1. *Prdm14*$^{-/-}$ E9.5 embryos have reduced PGC numbers with altered**
576 **distribution along the hindgut.** (A) Numbers of AP2γ-positive PGCs per
577 embryo across *Prdm14* genotypes. Means and confidence intervals are
578 shown. Kruskal-Wallis test was used for statistical comparison ($p<0.001$). (B)
579 Linear regression of AP2γ-positive PGC-numbers versus developmental stage
580 (somite number). R square values for *Prdm14* +/+, +/- and -/- embryos were
581 0.659, 0.514 and 0.001, respectively. (C) Image of a E9.5 mouse embryo with
582 PGCs (drawn green dots) migrating along the hindgut divided into four
583 quadrants (Q1 – Q4). Scale bar: 250 μm. (D) Distribution of PGCs along the
584 hindgut across *Prdm14* genotypes.

585

586 **Fig. 2. PRDM14 dosage controls global H3K27me3-levels in migrating**
587 **PGCs in both sexes.** (A) Representative images of AP2γ-positive PGCs with
588 upregulated and non-upregulated global levels of H3K27me3 across different
589 *Prdm14* genotypes (PGC-nuclei are outlined in H3K27me3 images). Scale
590 bar: 10 *μ*m. Intensity values for each channel along the yellow lines are
591 plotted on the right. (B) Percentages of H3K27me3-upregulated and non-
592 upregulated PGCs across *Prdm14* genotypes in male and female embryos.
593 (C) Percentages of H3K27me3 upregulated and non-upregulated PGCs at
594 different developmental stages (somite number). Labels in each column
595 indicate number of PGCs analyzed. Chi-square test was used for statistical
596 comparisons ($p<0.001$).

597

598 **Fig. 3. Erasure of H3K27me3-enrichment from the inactive X-**
599 **chromosome in migrating female PGCs is dependent on PRDM14.** (A)
600 Representative images of AP2γ-positive PGCs with presence or absence of
601 H3K27me3-accumulation (H3K27me3 spot, white arrowheads) on the inactive
602 X-chromosome. PGC-nuclei are outlined in the H3K27me3 channel. Scale
603 bar: 10 *μ*m. (B) Percentage of H3K27me3 spot-positive and -negative PGCs

604 across *Prdm14* genotypes. Labels in each column indicate number of cells
605 analyzed. (C) Erasure of the H3K27me3-spot in PGCs of different *Prdm14*
606 genotypes during their migration along the hindgut divided in four quadrants
607 (Q1-Q4). Labels in each column indicate number of PGCs analyzed. Chi-
608 square test was used for statistical comparisons ($p<0.001$).
609
610 **Fig. 4. Changes in both X-chromosomal and global levels of H3K27me3**
611 **in female PGCs require PRDM14 but are independent of each other.** (A)
612 Relationship between X-chromosomal (bar graphs, % of PGCs per genotype)
613 and global (pie charts, % of PGCs per genotype within each H3K27me3
614 spot/no spot sub-category) levels of H3K27me3 in PGCs from female
615 embryos of different *Prdm14* genotypes. Chi-square test was used to
616 compare dependency of global of H3K27me3 upregulation on X-chromosomal
617 removal for each *Prdm14* genotype (n.s., not significant; $Prdm14^{+/+}$ p=0.956,
618 $Prdm14^{+/-}$ p=0.499, $Prdm14^{-/-}$ p=0.110). (B) Schematic summary of *Prdm14*
619 genotype effect on global and X-chromosomal H3K27me3 reprogramming in
620 mouse PGCs.

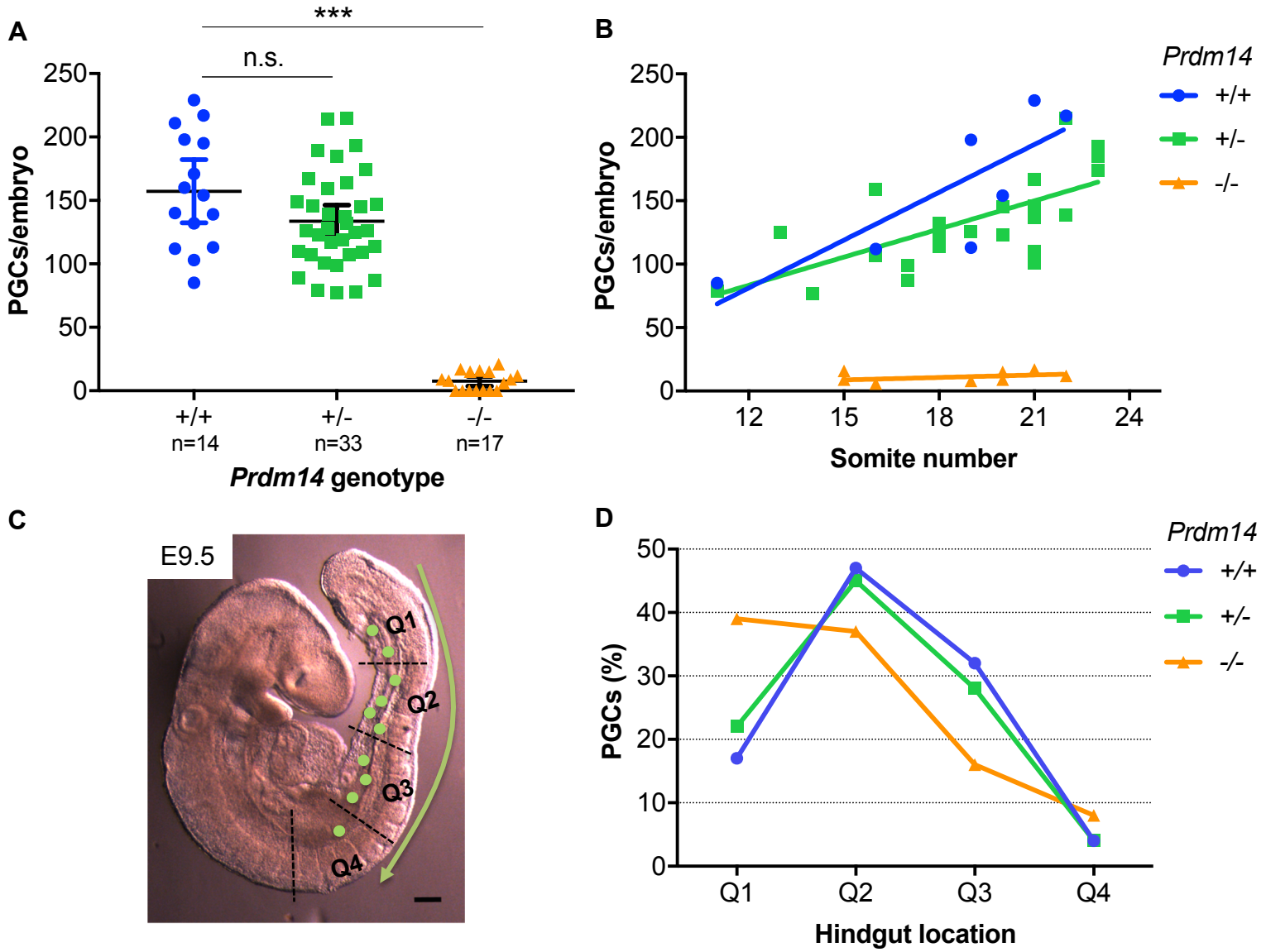
A
***
n.s.
PGCs/embryo
250
200
150
100
50
0
+/+
n=14
+/-
n=33
-/-
n=17
Prdm14 genotype
B
Prdm14
+/+
+/-
-/-
PGCs/embryo
12
15
18
21
24
Somite number
C
E9.5
Q1
Q2
Q3
Q4
D
Prdm14
+/+
+/-
-/-
PGCs (%)
50
40
30
20
10
0
Q1
Q2
Q3
Q4
Hindgut location

Figure 1

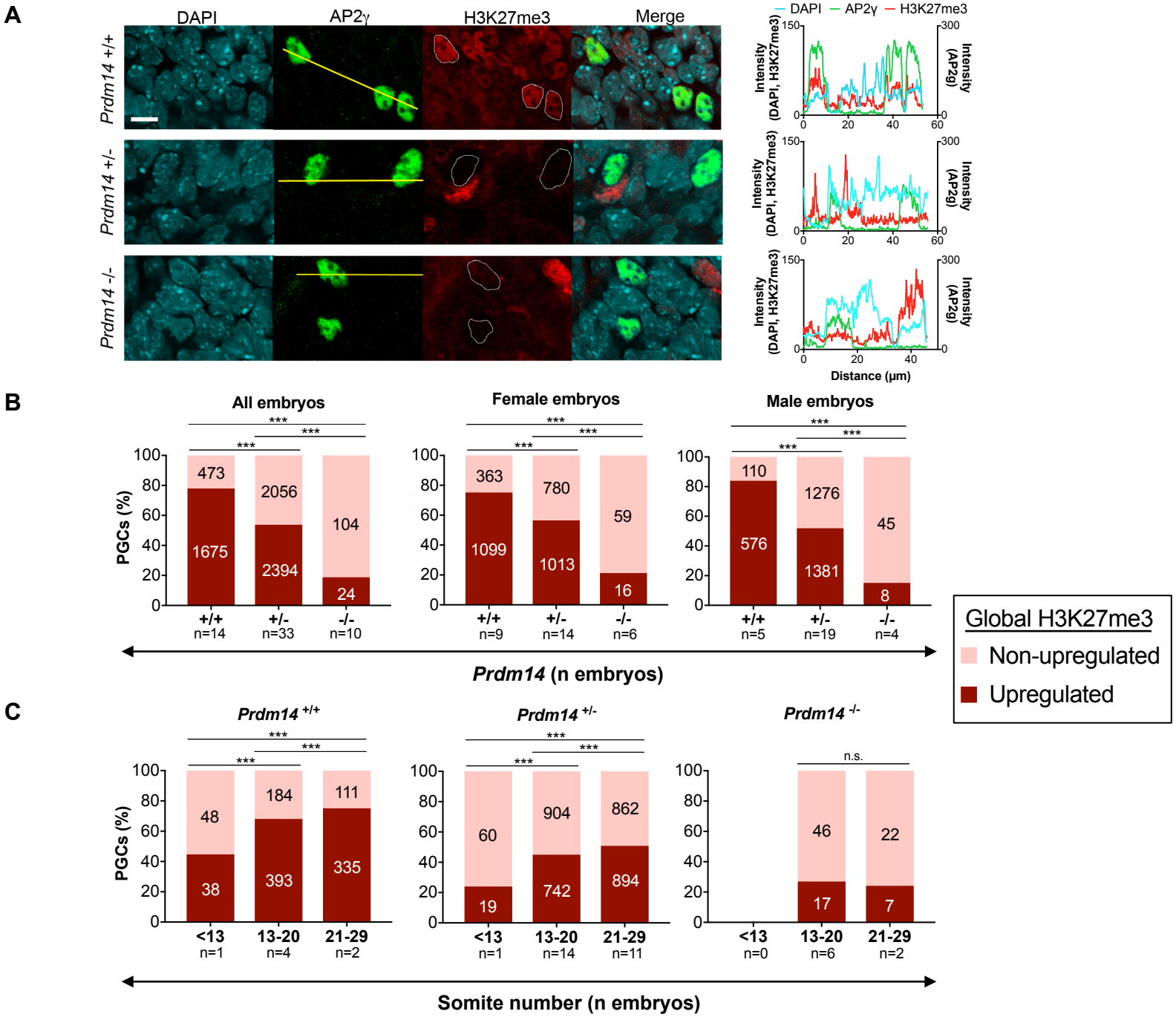
A
DAPI
AP2γ
H3K27me3
Merge
Prdm14 +/+
Prdm14 +/-
Prdm14 -/-
DAPI AP2γ H3K27me3
Intensity (DAPI, H3K27me3)
Intensity (AP2g)
Distance (µm)
B
All embryos
Female embryos
Male embryos
PGCs (%)
473
2056
104
1675
2394
24
363
780
59
1099
1013
16
110
1276
45
576
1381
8
+/+ n=14
+/- n=33
-/- n=10
+/+ n=9
+/- n=14
-/- n=6
+/+ n=5
+/- n=19
-/- n=4
Prdm14 (n embryos)
Global H3K27me3
Non-upregulated
Upregulated
C
Prdm14 +/+
Prdm14 +/-
Prdm14 -/-
n.s.
48
184
111
38
393
335
60
904
862
19
742
894
46
22
17
7
<13 n=1
13-20 n=4
21-29 n=2
<13 n=1
13-20 n=14
21-29 n=11
<13 n=0
13-20 n=6
21-29 n=2
Somite number (n embryos)

Figure 2

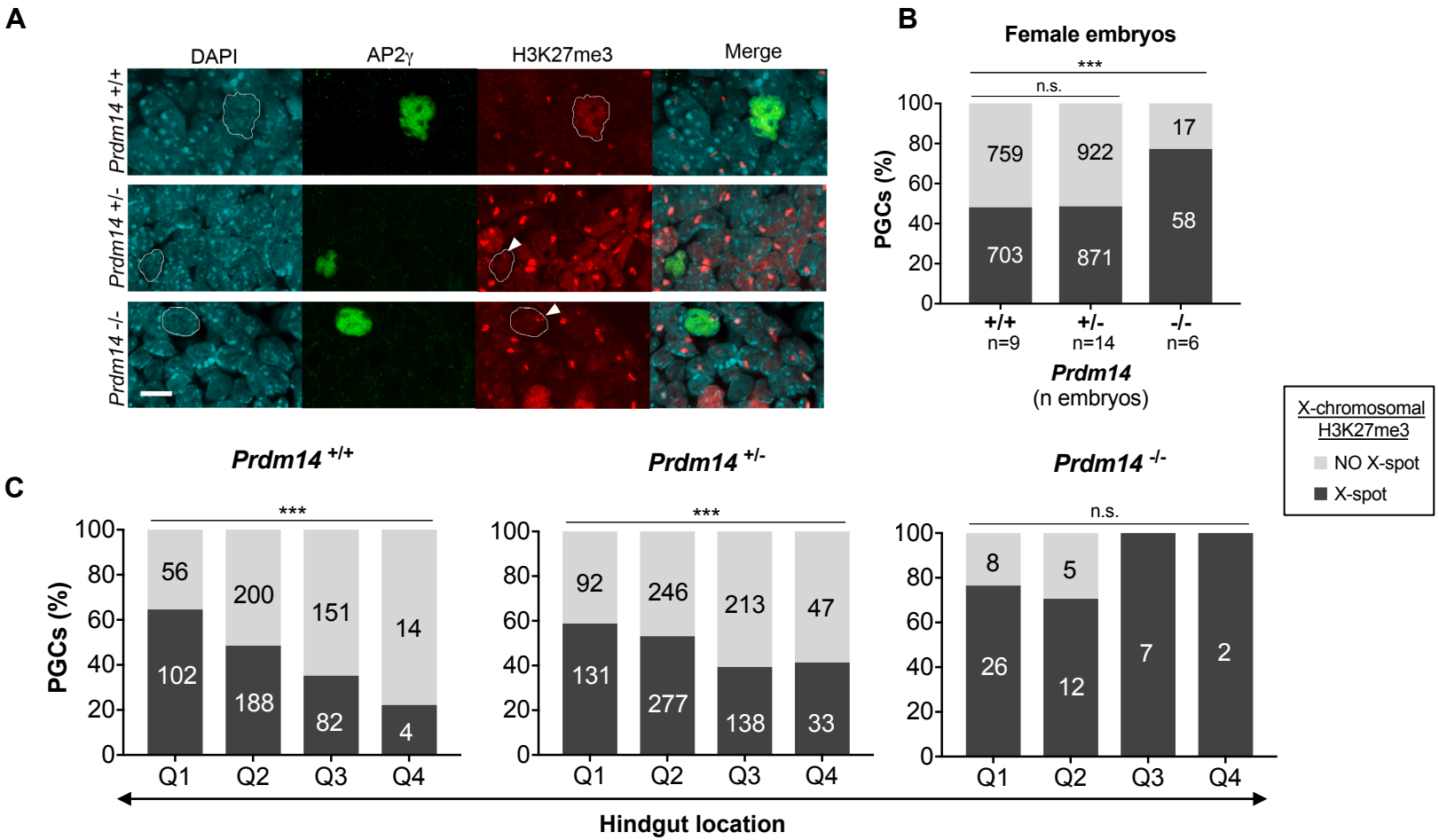
A
DAPI
AP2γ
H3K27me3
Merge
Prdm14 +/+
Prdm14 +/-
Prdm14 -/-
B
Female embryos
***
n.s.
PGCs (%)
759
922
17
703
871
58
+/+
n=9
+/-
n=14
-/-
n=6
Prdm14
(n embryos)
X-chromosomal H3K27me3
NO X-spot
X-spot
C
Prdm14 +/+
Prdm14 +/-
Prdm14 -/-
56
200
151
14
102
188
82
4
92
246
213
47
131
277
138
33
8
5
26
12
7
2
Q1
Q2
Q3
Q4
Hindgut location

Figure 3

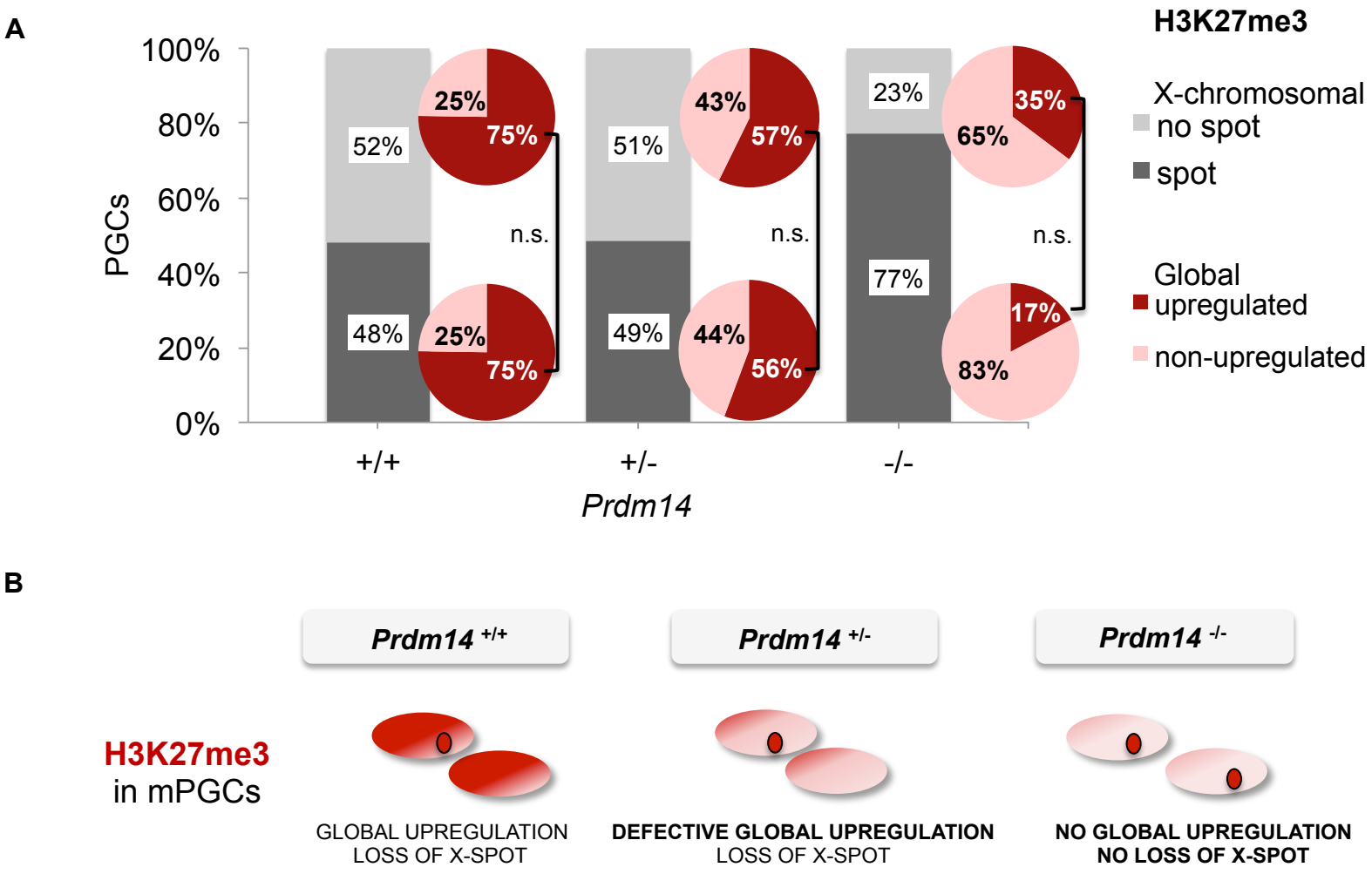
A
H3K27me3
100%
80%
60%
40%
20%
0%
PGCs
52%
48%
25%
75%
25%
75%
n.s.
51%
49%
43%
57%
44%
56%
n.s.
23%
77%
35%
65%
17%
83%
n.s.
+/+
+/-
-/-
Prdm14
X-chromosomal
no spot
spot
Global
upregulated
non-upregulated
B
Prdm14 +/+
Prdm14 +/-
Prdm14 -/-
H3K27me3
in mPGCs
GLOBAL UPREGULATION
LOSS OF X-SPOT
DEFECTIVE GLOBAL UPREGULATION
LOSS OF X-SPOT
NO GLOBAL UPREGULATION
NO LOSS OF X-SPOT

Figure 4